PHYSICAL REVIEW C VOLUME 23, NUMBER 1 JANUARY 1981

Radiative capture reaction ^{3}He(α,γ)^{7}Be at low energies

B. T. Kim,* T. Izumoto, and K. Nagatani
Cyclotron Institute, Texas A&M University, College Station, Texas 77843

(Received 25 August 1980)

The radiative capture reaction ^{3}He(α,γ)^{7}Be at low energies has been analyzed on the basis of the direct capture model in order to provide a theoretical estimate of the stellar reaction rate. The scattering wave functions of ^{3}He by α and the bound state wave functions of ^{7}Be were constructed by the empirical model, the phenomenological Woods-Saxon potential model, and the orthogonality condition model; these models account for the measured elastic scattering and excitation energies of the low-lying states of ^{7}Be. The total cross section factors $S(E_{\mathrm{c.m.}})$ of the $E1$, $M1$, and $E2$ capture from the $l = 0$–3 partial waves clearly show a rising behavior as the incident energy goes lower, which agrees with the experimental data. The negative scattering phase shifts, which can be associated with the presence of almost energy-independent inner oscillations in the relative wave function between ^{3}He and α due to the Pauli exclusion principle, seem to be responsible for this behavior.

[NUCLEAR REACTIONS ^{3}He $(\alpha,\gamma)^7$Be at low energies; direct capture model analysis; othogonality condition model; calculated $\sigma(E)$, $S(E)$, and branching ratios.]

I. INTRODUCTION

The radiative capture reaction ^{3}He$(\alpha,\gamma)^7$Be at low energies has attracted much attention to learning about the nonresonant direct capture mechanism and applying the result to the termination of the proton-proton chain stellar reaction. This reaction is particularly interesting because of the long-standing solar neutrino problem. The detection of the solar neutrinos by Davis *et al.*[1] is most sensitive[2] to the neutrino from the ^{8}B decay, which is produced directly by the proton capture on ^{7}Be formed from this reaction. The observed solar neutrino flux is smaller by a factor of about 3 than that predicted with known nuclear reaction rates. Over the past decade, this solar neutrino problem has motivated many experimental and theoretical attempts to understand this missing strength.

Recently, an experimental attempt[3] to measure the ^{3}He$(\alpha,\gamma)^7$Be reaction down to $E_{\mathrm{c.m.}} \approx 100$ keV has been made using techniques improved through their use in previous experiments.[4,5] The new results (triangles in Figs. 1 and 2) showed definitely smaller cross sections at low energy regions than the previous measurements (circles), which favors an observed smaller solar neutrino flux but seems to disagree with a theoretical prediction made by Tombrello and Parker.[6] Therefore, we consider it very important to reexamine in detail the theoretical calculation.

The total cross sections of the ^{3}He$(\alpha,\gamma)^7$Be reaction at low energies can be well described by the direct capture model.[6,7] The use of this model may be justified because there is no resonant state at lower energies than 4.57 MeV in ^{7}Be. Although the calculation for this model is quite straightforward, uncertainties lie in describing the wave functions for the relative motion between ^{3}He and α and the final ^{7}Be wave functions. The ^{3}He$+\alpha$ cluster approximation, ignoring p-Li and other cluster components in the ^{7}Be nuclear wave function, may be useful in describing the reactions performed at low energies of less than a few MeV. This clustering nature is suggested by these facts: (1) The ^{3}He$+\alpha$ structure is quite stable and binds together with only 1.58 MeV in the ground state; (2) the $\frac{7}{2}^-$ excited state at 4.57 MeV is known to be the f-wave resonant state decaying to ^{3}He and α; and (3) the p, n, and d separation energies from ^{7}Be are much larger than that for α. In fact, Tombrello and Parker[6] made use of the Whittaker function for the bound states of ^{7}Be in which amplitudes were adjusted to reproduce the experimental branching ratios and the observed total cross sections. The scattering waves were obtained from a hard-core potential which reproduces experimental elastic scattering phase shifts.

Our concern in this paper is to represent the improved wave functions by using a more reasonably attractive potential instead of a hard-core potential[6] between clusters and by including the effect of the Pauli principle in the orthogonality condition model (OCM).[8] This model is based on a microscopic description, and it is also best suited to treat a clustering pheonmenon just as the resonating group method[9,10] does. The asymptotic behavior of new wave functions should explain the low-energy ^{3}He$+\alpha$ elastic scattering data and the low-lying energy levels of ^{7}Be. We also attempt to give a theoretical limit for the direct capture cross sections at very low bombarding energies of astrophysical interest.

We reformulate the radiative direct capture cross sections with the first order perturbation theory in Sec. II. In this section a brief introduction of OCM is also given. In Sec. III we present the details of our model calculations. The physical aspects of our numerical results are discussed in order to give the limit of stellar reaction rates in Sec. IV. Finally, Sec. V presents our conclusions.

II. FORMALISM

A. Radiative direct capture theory

The interaction Hamiltonian[11] responsible for the radiative capture reaction is

$$H_{\text{int}} = -\frac{1}{c}\int \vec{j}\cdot\vec{A}\, d\vec{r}\,, \tag{1}$$

where $\vec{j}$ is the nuclear-current density and $\vec{A}$ is the vector potential in the radiation gauge, i.e., div $\vec{A}=0$. In the first-order perturbation theory, the radiative direct capture cross section of the reaction $A(\alpha,\gamma)B$ can be written in terms of the transition amplitudes as

$$\frac{d\sigma}{d\Omega_\gamma} = 2\left(\frac{e^2}{\hbar c}\right)\left(\frac{mc^2}{\hbar c}\right)\left(\frac{k_\gamma}{k_a}\right)^3 \frac{1}{2I_A+1}\sum_{M_B M_A \sigma} |T_{M_B M_A \sigma}|^2\,, \tag{2}$$

where k and k_γ denote the wave numbers of the incident channel and the emitted gamma rays, respectively, and m is the reduced mass of the incident channel. $I_A(M_A)$ stands for the spin (its projection) of nucleus A and σ for the polarization of the radiation, i.e., $\sigma=\pm1$. In the long wavelength limit, the transition amplitude can be expanded in terms of d functions with the electromagnetic multipole λ as

$$T_{M_B M_A \sigma}(\theta) = \sum_\lambda T^\lambda_{M_B M_A \sigma} d^\lambda_{M_A - M_B, \sigma}(\theta)\,, \tag{3}$$

where $\vec{k}_a$ is taken to be parallel to the z axis and Θ is the polar angle of $\vec{k}_\gamma$. We further decompose the electromagnetic multipole transition amplitude $T^\lambda_{M_B M_A \sigma}$ in terms of partial waves $l_a j_a$:

$$T^\lambda_{M_B M_A \sigma} = \sum_{l_a j_a} [\beta^{E\lambda}_{l_a j_a} + (-)^{\delta(\sigma+1)}\beta^{M\lambda}_{l_a j_a}] \times (l_a 0 I_A M_A | j_a M_A)(\lambda M_A - M_B I_B M_B | j_a M_A)\,. \tag{4}$$

For the $E1$, $M1$, and $E2$ transitions, which play an important role in the low-energy capture processes, the β's are

$$\beta^{E\lambda}_{l_a j_a} = i^{l_a} C(E\lambda)\hat{l}_a \hat{l}_b \hat{I}_B (l_b 0 \lambda 0 | l_a 0) \times W(\lambda l_b j_a I_A; l_a I_B) I^\lambda_{l_b I_B,\, l_a j_a}\,, \tag{5}$$

where l_b is the orbital angular momentum of $A+a$ two clusters in the nucleus B, and

$$C(E1) = im\left(\frac{Z_a}{m_a} - \frac{Z_A}{m_A}\right), \tag{6}$$

$$C(E2) = \frac{k_\gamma}{12} m^2\left(\frac{Z_a}{m_a^{\,2}} + \frac{Z_A}{m_a^{\,2}}\right), \tag{7}$$

and

$$\beta^{M\lambda}_{l_a j_a} = i^{l_a}\hat{l}_a \hat{l}_b \hat{I}_B \delta_{l_a l_b}\left[\frac{m\hbar c}{2m_p c^2}\left(\frac{Z_a}{m_a^{\,2}} + \frac{Z_A}{m_A^{\,2}}\right)[l_a(l_a+1)]^{1/2} W(1 l_a j_a I_A; l_a I_B) + \frac{\hbar c}{2m_p c^2}\mu_A (-)^{I_B - j_a}\hat{I}_A W(1 I_A j_a l_a; I_A I_B)\right] I^0_{l_b I_B,\, l_a j_a}\,, \tag{8}$$

where μ_A and Z_A are the magnetic moment and charge of A, respectively. The overlap integral I^λ is

$$I^\lambda_{l_b I_B,\, l_a j_a} = \int dr\, U_{l_b I_B}(r) r^\lambda \chi_{l_a j_a}(r)\,, \tag{9}$$

where $\chi_{l_a j_a}$ is the radial distorted wave and $U_{l_b I_B}$ the radial part of the bound state wave function. We chose the normalizations of these wave functions used by Tamura.[12] Numerical evaluation of the radial integral is necessary to obtain the cross sections after a model is adopted to describe the relative motion between A and a.

Since the capture cross sections $\sigma(E)$ at low energies rapidly decrease mainly due to the Coulomb penetrability, it is convenient to use the Coulomb-factored-out cross section $S(E)$, the so-called S factor, defined by

$$\sigma(E) = S(E)\exp(-2\pi\eta)/E\,, \tag{10}$$

where η is the Sommerfeld parameters and E is the incident energy in the center of the mass system.

B. Orthogonality condition model (OCM)

Microscopic studies[9,10] on interactions between clusters showed that the Pauli effects are very important. The role of exchange effects between clusters can be understood[8] in terms of the OCM, which excludes forbidden states due to the Pauli principle. This model gives a good agreement with the result of the resonating group method[9,10] which starts with a microscopic many-body Hamiltonian and takes into account a complete antisymmetrization.

The antisymmetrized ^{3}He $+\alpha$ cluster wave function is represented by vectors

$$\phi_{lj}=1\Big/\left[\binom{7}{3}\right]^{1/2}\mathcal{A}[h_{lj}\chi_{lj}] \tag{11}$$

with the channel wave function

$$h_{lj}=\phi(\alpha)[Y_l\times\phi_I(^3\mathrm{He})]_j, \tag{12}$$

where ϕ's are internal wave functions of two clusters, $\mathcal{A}$ is an antisymmetrizer between nucleons in two clusters, and χ is a radial function for the relative motion. χ is called a forbidden state (FS) when Eq. (11) is identically zero. The integral equation for χ^{FS} can be obtained by multiplying h_{lj} in Eq. (11) and by integrating over all internal coordinates as follows:

$$(1-K)\chi^{\mathrm{FS}}=0, \tag{13}$$

where the overlap kernel K is

$$K(r_1,r_2)=\frac{\delta(r_1-r_2)}{r_1r_2}-\left\langle h_{lj}\frac{\delta(r-r_1)}{r^2}\right|\left.\mathcal{A}h_{lj}\frac{\delta(r-r_2)}{r^2}\right\rangle. \tag{14}$$

Hence, χ^{FS} is the eigenfunction of K with the eigenvalue of unity in the following equation,

$$K\chi=\lambda\chi. \tag{15}$$

If we suppose ^{3}He and α consist of only s-wave nucleons with a common oscillator parameter ν, then the eigenfunctions of K (Refs. 9, 13) are always harmonic oscillator functions with an oscillator quantum number N and an oscillator parameter $(\frac{12}{7})\nu$. The eigenvalues, then, are

$$\lambda_N=3(\tfrac{5}{12})^N-3(-\tfrac{1}{6})^N+(-\tfrac{3}{4})^N. \tag{16}$$

The OCM excludes χ^{FS} by using the overlap kernel K and by solving the following equation for χ_{lj} in the matrix form[8,14]:

$$(1-K)^{1/2}(T_l+V^{\mathrm{eff}}-E)(1-K)^{1/2}\chi_{lj}=0, \tag{17}$$

where

$$T_l=\langle Y_l|T|Y_l\rangle \tag{18}$$

and T is a relative kinetic energy between clusters. The effective local potential V^{eff} is usually the direct folding potential and may be modified if necessary. The nonlocal potential $(1-K)^{1/2}V^{\mathrm{eff}}(1-K)^{1/2}$ is expected to include the contributions not only from the direct process but also from the exchange of nucleons. The radial wave functions χ_{lj} for the scattering states are normalized to an incident wave of unit flux while the bound state U_{lI} are taken as

$$\langle\phi_{lI}|\phi_{lI}\rangle=\langle U_{lI}|1-K|U_{lI}\rangle=1. \tag{19}$$

Assuming that the multipole operators of electromagnetic transition conserve the orbital symmetry of the internal wave functions of ^{3}He and α (Ref. 15) and that ^{3}He and α are made of s-wave nucleons, the matrix elements of the multipole operators in OCM can be obtained in exactly the same form as Eq. (4) except that the overlap integral of Eq. (9) becomes

$$I^{\lambda}{}_{l_bI_B,\,l_aj_a}=\langle(1-K)^{1/2}U_{l_bI_B}|r^{\lambda}|(1-K)^{1/2}\chi_{l_aj_a}\rangle. \tag{20}$$

In Ref. 15 a slightly different expression was used for which we have checked the numerical equivalence.

III. MODEL CALCULATIONS

The total capture cross section of the reaction ^{3}He$(\alpha,\gamma)^7$Be is a sum of cross sections leading to the $\frac{3}{2}^-$ ground state and $\frac{1}{2}^-$ excited state in ^{7}Be. Throughout our calculations, we only considered $E1$, $M1$, and $E2$ capture from $l=0-3$ partial waves. The magnetic moment of ^{3}He used was $-2.13\ \mu_N$. Since we were interested in very low energies, we were obliged to carry out the integration to a large radial distance of 50 – 80 fm in order to ensure the accuracy of our calculations. We also had to be careful in generating accurate Coulomb functions for large η and at large radial distance. For the present calculations, we adopted a computer program[16] which calculates the Coulomb wave functions with the high accuracy of at least 10^{-6}. We now introduce three different approaches in describing the relative motion between ^{3}He and α.

A. Empirical approach

The scattering wave $\chi_{l_aj_a}$ in Eq. (9) was obtained by using the hard-core repulsion in order to reproduce the low-energy experimental phase shifts. The bound state wave function $U_{l_bI_B}$ was chosen to be the Whittaker function associated with the proper separation energy. Its normalization was adjusted to explain both the experimental total cross sections and the gamma branching ratios between $\frac{3}{2}^-$ ground and $\frac{1}{2}^-$ excited states. This is essentially the same as Tombrello and Parker's calculations.[6] We therefore summarize very briefly the procedures of the calculations as follows.

(1) The empirical approach uses the hard-core potential to obtain the distorted waves. The s and d-wave nuclear phase shifts were nicely reproduced

by the hard-core potential with a nuclear radius of 2.8 fm. The *p* and *f*-wave phase shifts for the center of mass energy greater than 1.5 MeV were directly chosen as experimental phase shifts. For less than 1.5 MeV, where the observed values were not available, the hard-core phase shifts were multiplied by a factor of 6 in order to make smooth phase shifts in the entire energy range considered. The phase shifts obtained are compared with the measured values[17] in Fig. 4.

(2) The ^{7}Be bound state wave functions were assumed to be the Whittaker function with normalization factors of 1.25 for the ground state and 1.05 for the first excited state. These normalizations were chosen so that the calculated cross sections would reproduce the observed total cross sections and the branching ratios between the transitions to the ground and first excited states.

The calculated total cross sections $\sigma(E)$, cross-section factors $S(E)$, and branching ratios are shown in Figs. 1, 2, and 3, respectively, where three sets of experimental data are also displayed.[3-5] The data of Nagatani *et al.*[5] and Rolfs[3] are only plotted for low energies less than 300 keV. The Rolfs' data are normalized at 1500 keV. The theoretical cross sections, represented as dotted lines in the figures, reproduce the data of Parker and Kavanagh,[4] and Nagatani *et al.*,[5] and also confirm the previous calculation of Tombrello and Parker.[6] The calculated branching ratios have a slight energy dependence, but this could not be experimentally proved because of the large variations in the observed values.

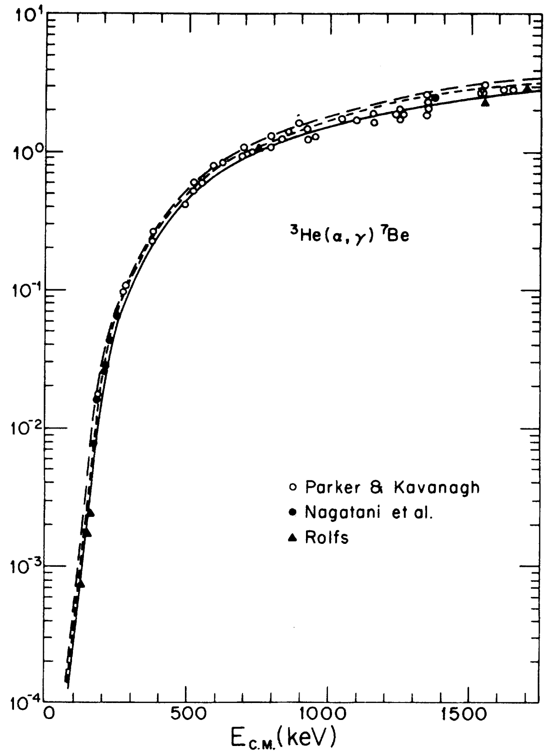

FIG. 1. The calculated total capture cross sections of ^{3}He(α,γ)^{7}Be as a function of the center-of-mass energy. The dotted, solid, and dashed curves are the theoretical predictions from the empirical approach, the Woods-Saxon potential approach, and the OCM approach, respectively. The data are obtained from Refs. 3, 4, and 5.

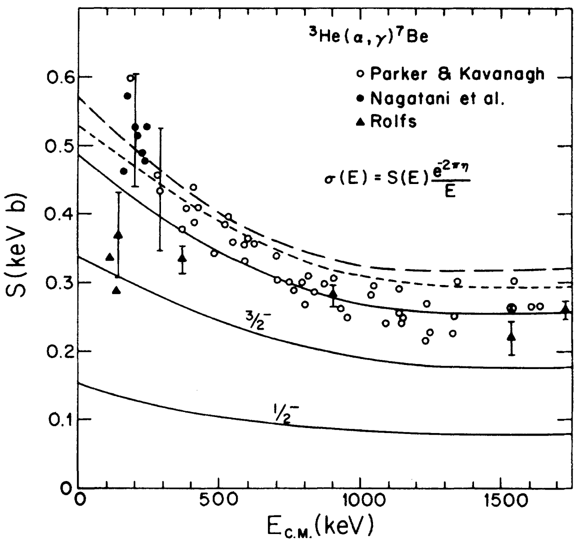

FIG. 2. The calculated S factors of ^{3}He(α,γ)^{7}Be. Otherwise the same as in Fig. 1. The S factors leading to the $\frac{3}{2}^-$ ground and $\frac{1}{2}^-$ excited states obtained from the Woods-Saxon potential approach are also shown with the solid lines.

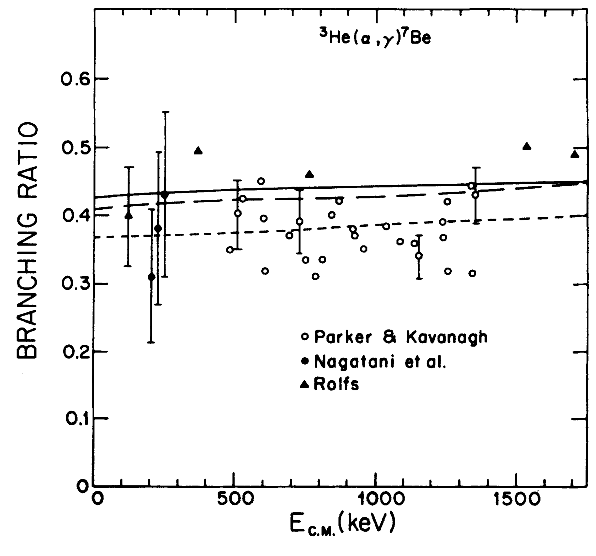

FIG. 3. The energy dependence of the branching ratios. Otherwise the same as in Fig. 1.

B. Phenomenological potential approach

We attempt to construct a parity dependent, local potential of the Woods-Saxon type with a reasonable geometry which accounts for the binding energies of low-lying states in ^{7}Be and low-energy elastic scattering data. The potential is found to be attractive, which contrasts with the previous hard-core approach. The coupling with reaction channels is neglected, and thus the potential is real. Unfortunately, there is no guiding principle for choosing parameters. We started with the conventional bound state problem to obtain the experimental separation energies of the ground and first excited states of ^{7}Be. Because of ambiguities in the shape of the nuclear potential, we still have continuous sets of parameters. We then imposed the restriction that the potential parameters should reproduce the position and width of the $f_{7/2}$ resonant state at 4.57 MeV and the measured total capture cross section. Care was taken to include this resonance since the tail of the resonance could have an influence on the low-energy cross section. We examined a parity-dependent potential (POT A), the geometries of which are $V_{\text{even}}=76.0$ MeV, $V_{\text{odd}}=93.85$ MeV, $V_{\text{s.o.}}=1.0$ MeV, $R_{\text{even}}=R_{\text{odd}}=R_{\text{s.o.}}=2.05$ fm, and $a_{\text{even}}=a_{\text{odd}}=a_{\text{s.o.}}=0.70$ fm. It reproduces well the experimental phase shifts (Fig. 4) and low-lying levels of ^{7}Be (Fig. 5). The calculated $\sigma(E)$, $S(E)$, and branching ratios with $\chi_{l_a j_a}$ and $U_{l_b I_B}$ generated by this potential are shown with the solid curves in Figs. 1, 2, and 3, respectively. We note again that $S(E)$ exhibits rising behavior as the beam energy goes lower. The branching ratios are very similar to those from the empirical approach.

C. Orthogonality condition model approach

The OCM calculation of the ^{3}He$+\alpha$ system have been performed by several authors.[18,19] We directly employed a potential suggested by Saito.[18] However, the potenital was slightly modified to include the spin-orbit force so that the splitting of the $\frac{3}{2}^-$ ground and $\frac{1}{2}^-$ excited states in ^{7}Be could be reproduced. The explicit form of the effective potential is, in the unit of MeV,

$$V_{\text{even}}=-103.38\exp(-0.2009r^2)$$
$$+13.78\exp(-0.0913r^2)+V_{\text{s.o.}},$$
$$V_{\text{odd}}=-88.00\exp(-0.1644r^2)+V_{\text{s.o.}},$$
$$V_{\text{s.o.}}=-1.60\frac{1}{r}\frac{d}{dr}\exp(-0.1644r^2)\vec{s}\cdot\vec{l}\,.$$

$\chi_{l_a j_a}$ and $U_{l_b I_B}$ were obtained by solving the OCM equation, Eq. (17), with this potential and by imposing appropriate normalizations and boundary conditions. The forbidden states with the eigenvalue $\lambda_N=$ in Eq. (15) were 0s and 1s for the s-wave, 0p for the p wave, and 0d for the d wave.

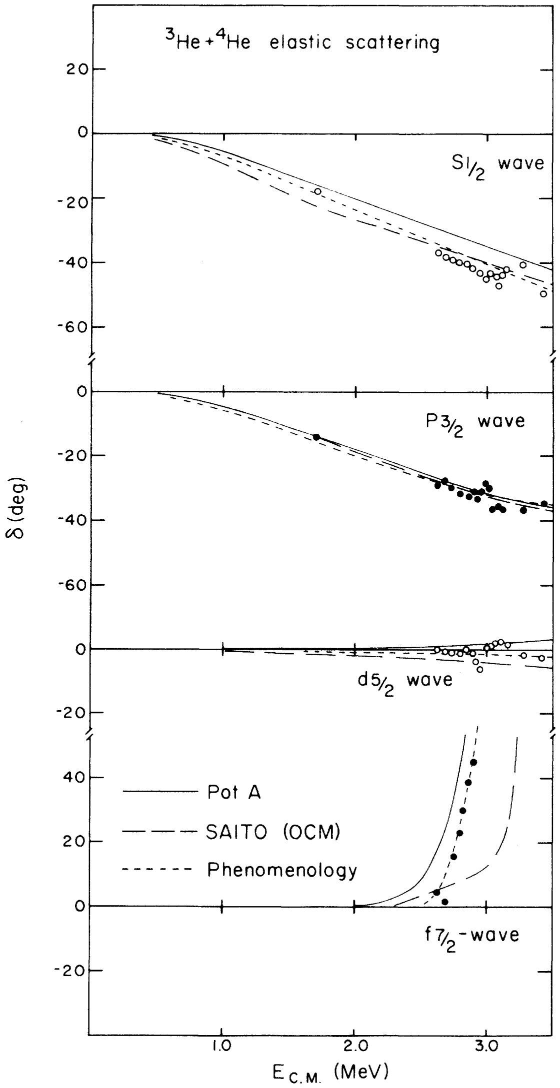

FIG. 4. Comparisons of the experimental and calculated phase shifts. The dotted, solid, and dashed curves indicate the theoretical values obtained from the hard-core potential with a nuclear radius of 2.8 fm, POT A, and Saito's potential in the OCM equation, respectively. The data are from Ref. 17.

The calculated elastic scattering phase shifts and low-lying states of ^{7}Be are displayed in Figs. 4 and 5, respectively. The direct capture cross sections and branching ratios obtained are shown with the dashed curves in Figs. 1, 2, and 3, respectively. The results obtained are very similar to the previous ones discussed in Secs. III A and III B. The total cross sections are larger by a factor of 1.2 than the measured ones. This is mainly because we assume the bound states in ^{7}Be are made of ^{3}He and α clusters [Eq. (19)]. In the

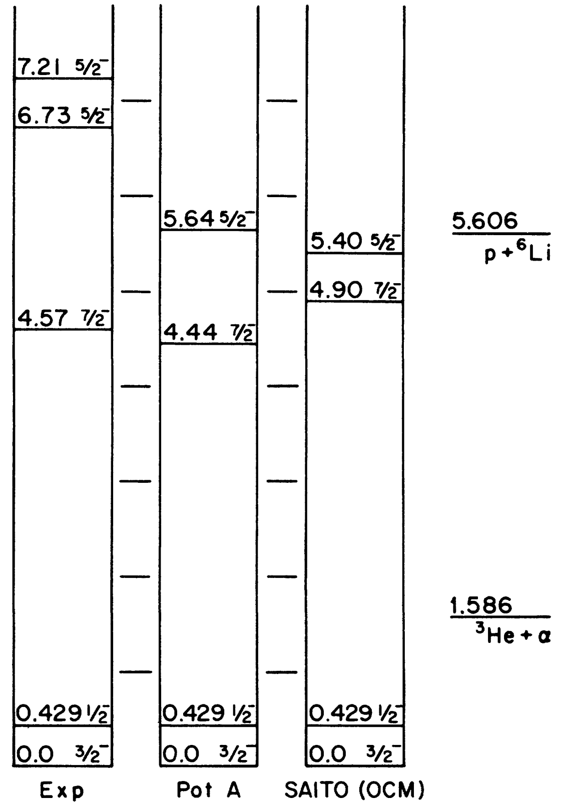

FIG. 5. The predicted low-lying level scheme of ^{7}Be from the POT A and OCM approaches along with the experimental one. The cluster threshold energies are also displayed.

calculation of the absolute cross section, we should thus multiply the wave function by the spectroscopic amplitude of this cluster configuration. Alternatively, in this comparison, the probability of the ^{3}He$+\alpha$ clustering in the bound states of ^{7}Be is the inverse of this factor, i.e., 1/1.2.

IV. DISCUSSION

The numerical results obtained from the three different approaches are basically the same, even though they start with quite different types of potential in generating the nulcear wave functions. The success of the empirical approach can be understood by examining OCM waves in detail. The orthogonality condition, excluding the forbidden states due to the Pauli principle, yields the almost energy-independent nodal points in the relative wave functions between ^{3}He and α clusters. We plot the $s_{1/2}$ and $p_{3/2}$ scattering wave functions from the OCM for $E_{\text{c.m.}}=0.1$ and 5.0 MeV in Fig. 6. The $p_{3/2}$ ground state wave function of ^{7}Be is also shown. It clearly demonstrates the almost energy-independent inner oscillation that gives rise to the inner repulsive effect. Furthermore, this characteristic leads to a unique shape of the overlap integral in the inner region for a given multipole capture. We display in Fig. 7 the real part of the radial overlap of the $E1$ capture from the s wave which was obtained in the POT A approach. There exists an almost energy-independent cutoff radius r_C where the

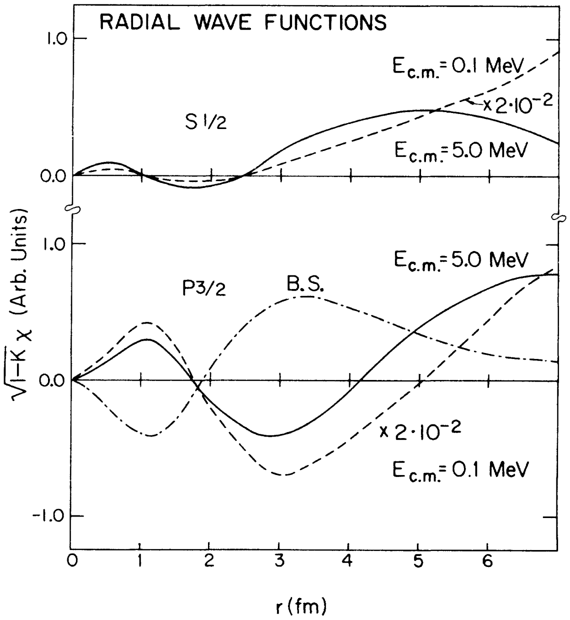

FIG. 6. The real part of the OCM radial wave function of the $s_{1/2}$ and $p_{3/2}$ waves for $E_{\text{c.m.}}=0.1$ and 5.0 MeV. The bound state wave function of the $\frac{3}{2}^-$ ground state is also plotted. The almost energy-independent inner oscillations are clearly shown.

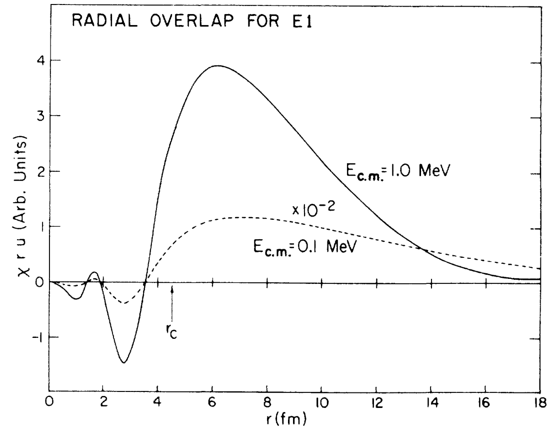

FIG. 7. The real part of the radial overlap for $E1$ from the s wave at $E_{\text{c.m.}}=0.1$ and 1.0 MeV obtained from the Woods-Saxon potential approach. The cutoff radius r_C, where integration over zero to r_C becomes zero, is shown to be almost energy independent.

overlap integral from $r=0$ to r_C becomes zero. The same characteristic was also obtained in the OCM calculation. It supports the use of the hard-core potential for the analysis. The existence of r_C further implies that the capture process taking place in the outer region only contributes to the measured cross sections, and that the asymptotic behaviors of wave function, i.e., the phase shifts of scattering wave and binding energies of ^{7}Be, play a vital role in estimating the cross section. The potentials employed for these three different approaches reproduce equally well the observed phase shifts (Fig. 4) and binding energies of ^{7}Be (Fig. 5), giving us the same results. The Pauli effect which was crucial to an understanding of the reaction process does not affect much the magnitude of the cross section since it corrects only the inner part of the wave function.

We now turn to discuss several physical aspects which we observed in the numerical results.

A. Multipole and partial wave contributions

In the reactions at low energies, the s wave dominates the scattering; therefore, the $E1$ capture should make a large contribution to the cross sections. This is clearly shown in Fig. 8 where we display each multipole and each partial wave contribution to the cross sections leading to the $\frac{3}{2}^-$ ground state from the Woods-Saxon potential model. The s-wave contribution is more appreciable when energy approaches zero, while the d wave becomes significant as energy goes higher. In the low energy region, $E1$ from the s wave and d wave is much larger than $E2$ from the p and f wave or $M1$ from the p wave. We note that all contributions are smooth over the entire energy region considered.

B. Anisotropy of radiation

If the s wave is dominant, the angular distribution of the radiation should be isotropic. Therefore, the effects from other partial waves in the reaction process can be clearly seen in the angular distribution. In the experimental measurements, the observed total cross sections were determined by assuming an isotropic radiation. We can predict the uncertainty based on this assumption from the theoretical angular distribution. We show several angular distributions at different energies in Fig. 9. At $E_{\text{c.m.}} = 50$ and 100 keV, there is a broad peak around 90° because of interference between the s- and d-wave contributions, which is characteristic of the $E1$ capture. However, as the incident energy goes higher, the $E2$ and $M1$ captures come in. The angular distributions lose a symmetry around 90° and show a slight backward-angle rise due to the constructive

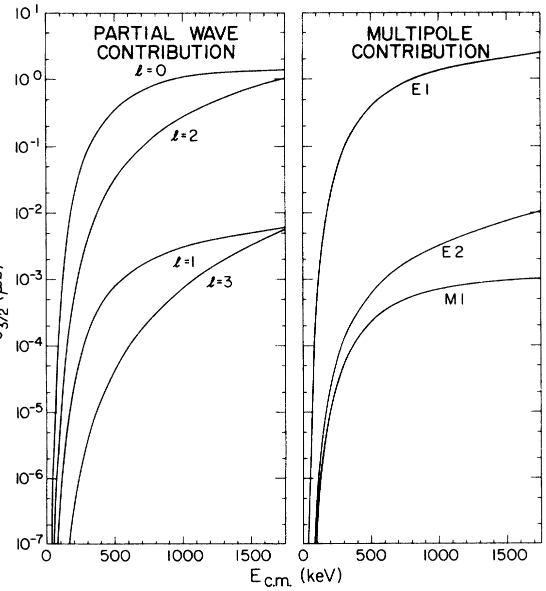

FIG. 8. Partial wave and multipole contributions to the capture cross section leading to the $\frac{3}{2}^-$ ground state obtained from the Woods-Saxon potential approach. The other approaches demonstrated very similar features.

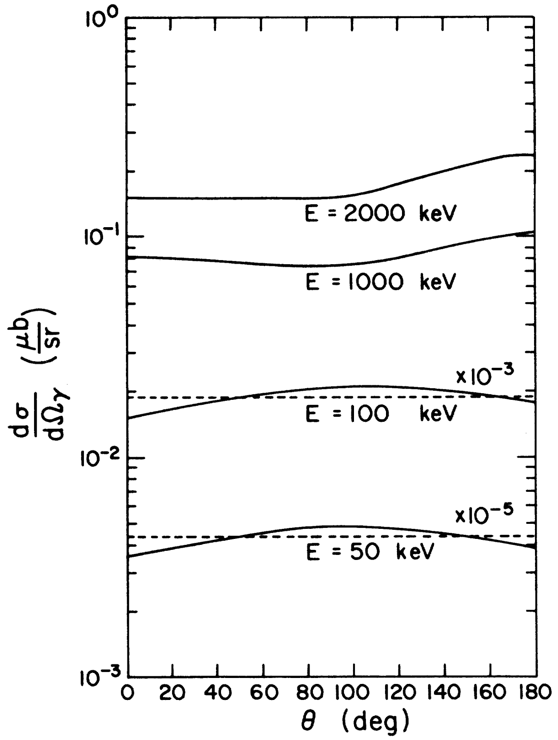

FIG. 9. Angular distributions of the capture cross section leading to the $\frac{3}{2}^-$ ground state obtained from the Woods-Saxon potential approach. The dashed lines show the isotropic s-wave contribution.

interference of $E2$ with $E1$. It is worth noting that the uncertainty of the total cross sections due to anisotropy in the energy range we calculated is at most 8%.

C. Branching ratio

The branching ratio comes mainly from the difference of the spin factor $2I_B+1$ and the binding energy of two final states $\Phi_{l_b I_B}$. The low energy Wentzel-Kramers-Brillouin (WKB) calculations[7] for the $E1$ capture from the s wave showed $S(\frac{1}{2}^-)/S(\frac{3}{2}^-) \approx E_B(\frac{1}{2}^-)/2E_B(\frac{3}{2}^-) \approx 0.37$, where E_B is the binding energy. In fact, the energy dependence of branching ratios is very weak, as seen in Fig. 3, and three different model calculations again give almost the same results.

D. Shape of $S(E)$

In order to obtain the S factors at very low energies, say several keV, of astrophysical interest, experimental S factors measured at higher energies are extrapolated using theoretical predictions. It is thus important to investigate the origin of the envelope of $S(E)$. Let us consider sider the $E1$ capture from the s wave which is a dominant process at very low energies. If we admit the hard-core potential with a radius r_C, the distorted wave for $l=0$ in the external region is

$$\chi_{0,1/2} = F_0 + e^{i\delta_0} \sin \delta_0 (G_0 + iF_0),$$

where δ_0 is the s-wave nuclear phase shift and F_0 and G_0 are the s-wave regular and irregular Coulomb function, respectively. The S factor then becomes

$$S = \left| \sqrt{S_F} + \tan \delta_0 \sqrt{S_G} \right|^2 \cos^2 \delta_0,$$

where

$$S_f = A \left| \int_{r_C}^{\infty} dr\, U r f \right|^2, \quad f = F_0 \text{ or } G_0.$$

A is the geometrical and dynamical factor for $E1$ due to the s wave in Eqs. (2) and (4). For the charged particle scattering at low energy, $\tan \delta_0$ is proportional[20] to $2\pi\eta k \exp(-2\pi\eta)$. The proportional constant has a very weak energy dependence. In Fig. 10, we plot $\sqrt{S_F}$ and $2\pi\eta k \exp(-2\pi\eta)\sqrt{S_G}$ versus $E_{\text{c.m.}}$ leading to the $\frac{3}{2}^-$ ground state (solid curves) and to the $\frac{1}{2}^-$ excited state (dotted lines). It is apparent that the negative phase shifts always make the S factor rise at a slope steeper than that of S_F as $E_{\text{c.m.}}$ approaches zero, while the shape of $S(E)$ with positive phase shifts can be determined by the magnitude of the phase shift. In other words, an S factor that is more flattened than S_F or even decreasing may be obtained only with the positive phase shifts. Hence, the shape of $S(E)$ at a low energy region depends largely on the sign of the phase shift. We also notice that the branching ratio with negative (positive) phase shift is bigger (smaller) than $S_F(\frac{1}{2}^-)/S_F(\frac{3}{2}^-)$ in the energy region considered.

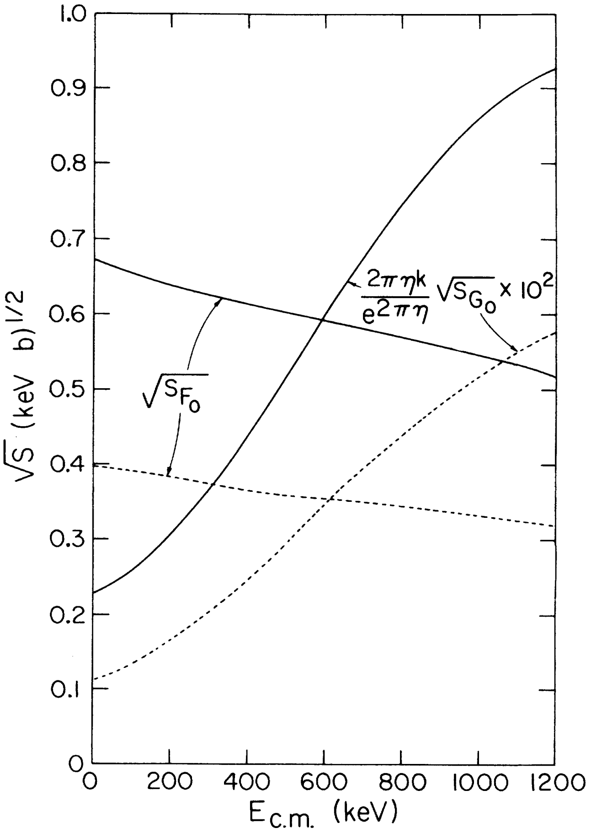

FIG. 10. $\sqrt{S_F}$ and $2\pi\eta k \exp(-2\pi\eta)\sqrt{S_G}$ versus $E_{\text{c.m.}}$. The solid and dotted curves are for the $\frac{3}{2}^-$ ground and $\frac{1}{2}^-$ excited states, respectively.

The question is whether we can assign the definite sign of the phase shift in the relative wave function. Our OCM study has shown that the exchange effects give rise to the almost energy-independent nuclear inner oscillation in the relative wave function between ^{3}He and α, this oscillation plays an equivalent role to a strong repulsive core in the effective potential. The hard-core always gives negative phase shifts as long as $r_C < \lambda\!\!\!^{-}$, where $\lambda\!\!\!^{-}$ is the wavelength in the incident channel. This is actually the present case. Experimental phase shifts were also shown to be negative. This result implies that the S factor's rise toward lower energies is essential.

E. Absolute value of S factor

We should admit that the absolute magnitude of the S factor cannot be uniquely determined from the approaches mentioned so far. Uncertainty arises with the ambiguity of the nuclear potential and the approximations made for the cluster treatment of the system, long-wavelength limit of the radiation, etc. The OCM approach using the Saito potential, which accounts very well for the scattering problem, overestimated the cross sections because the amplitude of the ^{3}He + α clustering configuration for ^{7}Be was assumed to be unity. The geometry of the nuclear potential was chosen so that various experimental facts were reproduced. However, it could not determine a unique potential. For example, if we use POT B without any orthogonality conditions, which reproduces experimental data with the same quality of fit as that with POT A and which has geometries of $V_{\text{even}} = 75.0$ MeV, $V_{\text{odd}} = 92.5$ MeV, $V_{\text{s.o.}} = 1.0$ MeV, $R_{\text{even}} = R_{\text{odd}} = R_{\text{s.o.}} = 2.15$ fm, and $a_{\text{even}} = a_{\text{odd}} = a_{\text{s.o.}} = 0.60$ fm, we obtain an S factor smaller by 20%. The accurately measured spectroscopic factor of the ^{3}He + α clustering, root-mean-square radius, and electromagnetic properties in ^{7}Be could reduce the uncertainties mentioned above. In the present approach, it is probably necessary to renormalize theoretical values to a measured capture cross section which is experimentally reliable.

V. CONCLUSIONS

We have analyzed the ^{3}He(α,γ)^{7}Be reaction at very low energies on the basis of the direct capture model in order to study the nonresonant direct capture reaction mechanism and to obtain stellar nuclear reaction rates. The ^{7}Be nuclear wave function and the distorted waves in the incident channel were constructed with (1) purely empirical elastic scattering data, (2) the phenomenological Woods-Saxon potential, and (3) the Saito potential in the OCM equation. In each approach, the reaction mainly proceeds through the $E1$ transition by means of the s wave in the low energy region. These approaches consistently show that the S factors rise as energy goes to zero, which agrees closely with the experimental data.[4,5] This behavior seems to be initiated by the negative phase shifts which can be explained by the presence of energy-independent inner oscillations due to the exchange effects in the relative motion between ^{3}He and α. Because of uncertainties in the ^{3}He + α clustering component in ^{7}Be and the nuclear potential geometry chosen, no approach gives an absolute value of reaction rates. If the theoretical values are normalized to the experimental value of $S = 0.275$ keV b at $E_{\text{c.m.}} = 1000$ keV, our three approaches yield $S(0) = 0.48 \pm 0.01$ keV b and $dS(0)/dE = (-2.9 \pm 0.2) \times 10^{-4}$ b.

This work was supported in part by the National Science Foundation.

---

*Present address: Sung Kyun Kwan University, Seoul, Korea.

[1] R. Davis, Jr., in Proceedings of the Informal Conference on Status and Future of Solar Neutrino Research, Brookhaven National Laboratory, 1978, edited by G. Friedlander, p. 1 (unpublished).

[2] J. N. Bahcall, N. A. Bahcall, and R. K. Ulrich, Astrophys. J. 156, 559 (1969). The present status of the solar neutrino problem is summarized in a recent article by J. N. Bahcall *et al.*, Phys. Rev. Lett. 45, 945 (1980).

[3] C. Rolfs, Proceedings of the International Workshop VII, Hirschegg, Austria, 1979 (unpublished).

[4] P. D. Parker and R. W. Kavanagh, Phys. Rev. 131, 2578 (1963).

[5] K. Nagatani, M. R. Dwarakanath, and D. Ashery, Nucl. Phys. A128, 325 (1969).

[6] T. A. Tombrello and P. D. Parker, Phys. Rev. 131, 2582 (1963).

[7] R. F. Christy and I. Duck, Nucl. Phys. 24, 89 (1961).

[8] S. Saito, Prog. Theor. Phys. 40, 893 (1968).

[9] H. Horiuchi, Prog. Theor. Phys. Suppl. 62, 90 (1977).

[10] Y. C. Tang, M. LeMere, and D. R. Thompson, Phys. Rep. 47, 167 (1978).

[11] A. DeShalit and H. Feshbach, *Theoretical Nuclear Physics* (Wiley, New York, 1974), Vol. 1, p. 667.

[12] T. Tamura, Phys. Rep. C14, 59 (1974).

[13] D. A. Zaikin, Nucl. Phys. A170, 584 (1971).

[14] B. Buck, H. Friedrich, and C. Wheatley, Nucl. Phys. A275, 246 (1977).

[15] Y. Suzuki, Prog. Theor. Phys. 55, 1751 (1976); 56, 111 (1976).

[16] A. R. Barnett, D. H. Feng, J. W. Steed, and L. J. B. Goldfarb, Comput. Phys. Commun. 8, 377 (1974).

[17] R. J. Spieger and T. A. Tombrello, Phys. Rev. 163, 964 (1967).

[18] S. Saito, Prog. Theor. Phys. Suppl. 62, 11 (1977).

[19] H. Friedrich, Nucl. Phys. A294, 81 (1978).

[20] C. Mahaux and H. A. Weidenmüller, *Shell Model Approach to Nuclear Reactions* (North-Holland, Amsterdam, 1969), p. 5.